LBL-19959
Preprint c.2

Lawrence Berkeley Laboratory
UNIVERSITY OF CALIFORNIA

Materials & Molecular Research Division

Submitted to Journal of the Electrochemical Society

DESIGN OF THIN-GAP CHANNEL FLOW CELLS

V. Edwards and J. Newman

August 1985

TWO-WEEK LOAN COPY
This is a Library Circulating Copy
which may be borrowed for two weeks.

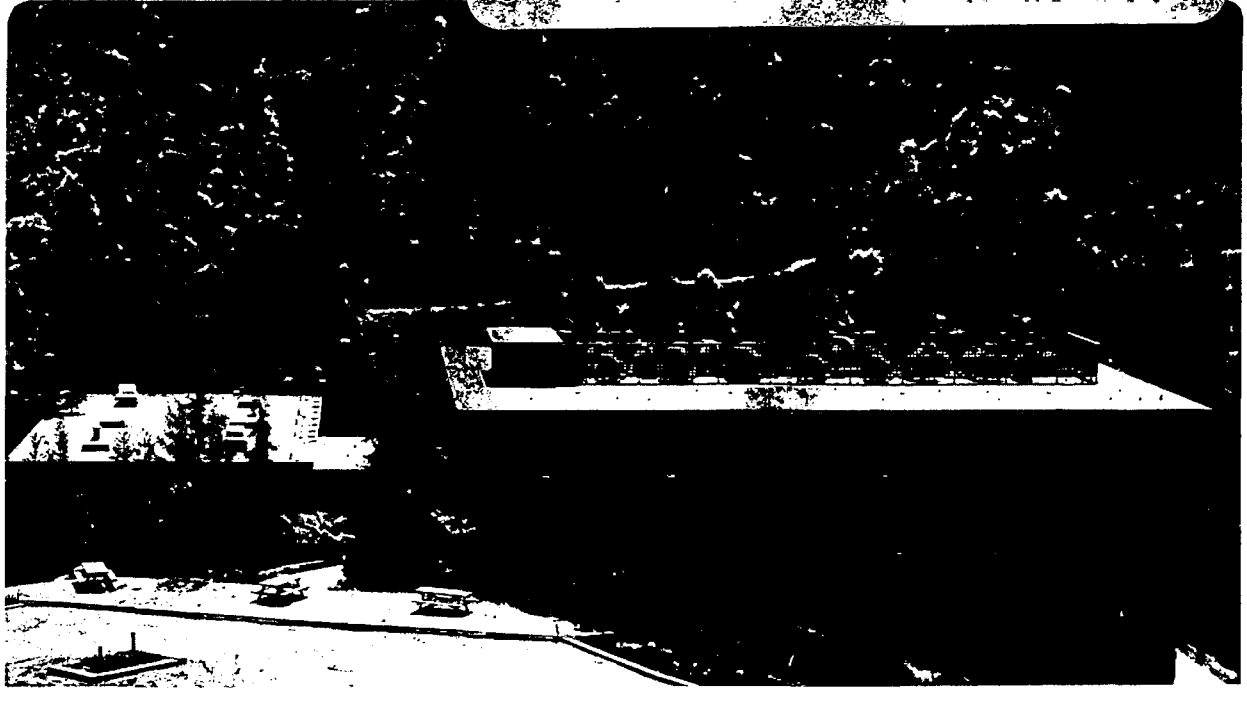

LBL-19959 c.2

Prepared for the U.S. Department of Energy under Contract DE-AC03-76SF00098

DISCLAIMER

This document was prepared as an account of work sponsored by the United States Government. While this document is believed to contain correct information, neither the United States Government nor any agency thereof, nor the Regents of the University of California, nor any of their employees, makes any warranty, express or implied, or assumes any legal responsibility for the accuracy, completeness, or usefulness of any information, apparatus, product, or process disclosed, or represents that its use would not infringe privately owned rights. Reference herein to any specific commercial product, process, or service by its trade name, trademark, manufacturer, or otherwise, does not necessarily constitute or imply its endorsement, recommendation, or favoring by the United States Government or any agency thereof, or the Regents of the University of California. The views and opinions of authors expressed herein do not necessarily state or reflect those of the United States Government or any agency thereof or the Regents of the University of California.

LBL-19959

Design of Thin-Gap Channel Flow Cells

Victoria Edwards* and John Newman**

Materials and Molecular Research Division, Lawrence Berkeley Laboratory, and

Department of Chemical Engineering, University of California,

Berkeley, California 94720

August 6, 1985

Abstract

A model for predicting the current, concentration, and potential distributions in a thin-gap channel flow cell is presented. The model does not invoke the thin-diffusion-layer assumption or the assumption of straight current lines, and it allows for multiple reactions. The model, however, does not include the effect of migration; thus, it is only valid for systems with excess supporting electrolyte. This model can be used for the design and scale-up of channel flow electrochemical reactors. Results are presented for a single reaction to show the effects of interacting diffusion boundary layers and of the axial component of current.

---

* Electrochemical Society Student Member

** Electrochemical Society Active Member

Key Words: undivided cells, current distribution, mass transfer

Introduction

A channel flow cell consists of two parallel plates, between which electrolytic solution flows. When the gap between the two plates is thin compared to the diffusion-boundary-layer thickness, the cell is called a thin-gap channel flow cell. The advantage of a thin-gap cell is its low ohmic drop.

The analysis of thin-gap cells is complex because several effects must be taken into account. For example, when the gap is thin, the boundary layers "interact" because the species can diffuse across the gap to the opposite electrodes. Although low-Reynolds-number channel flow cells have been analyzed by many investigators, *e.g.* (1-8), each model contains several simplifying assumptions. Here, we shall present a new model and discuss how the results are affected by the interaction of the diffusion boundary layers and by the axial component of current.

The model presented here is similar to those of White *et al.* (1) and Parrish and Newman (3). White's model accounts for interacting boundary layers, multiple heterogeneous and homogeneous reactions, and migration. His model, however, does not account for the two-dimensional structure of the potential distribution because it assumes that the current lines are straight (no net axial current). Parrish and Newman's model accounts for the two-dimensional potential distribution, but it is written for a single reaction, and it assumes that the diffusion boundary layers are thin, and, therefore, do not interact.

The model presented here does not assume thin diffusion boundary layers or straight current lines. The model, however, does not account for homogeneous reactions. It also assumes that there is excess supporting electrolyte; therefore, migration is neglected. Because the governing equations for this model are linear, the technique of superposition is used to reduce the problem from two-dimensional to one-dimensional.

After the assumptions and governing equations are presented, the results of the model will be discussed.

Geometry and Assumptions

Figure 1 shows the cell geometry. The fluid enters from the left in fully developed laminar flow. The electrochemical reactions occur on the electrode surfaces, and boundary layers (shown by the dotted lines) develop on each electrode. In the model, these boundary layers may touch the opposite electrodes.

The assumptions for the model are as follows: there are no homogeneous chemical reactions; the cell does not contain a separator; there is excess supporting electrolyte (migration can be neglected); the flow is laminar; and axial diffusion is negligible. For the flow to be laminar, the Reynolds number (based on $d_e=2h$) must be less than 2100 (9). For negligible axial diffusion, the Péclet number must be greater than about 10. This assumption is generally valid because Pe=ReSc, where Sc is typically 1000 for electrochemical systems.

Governing Equations

Table I lists by name the governing equations and the corresponding unknowns. At the left of each column is the number of equations or unknowns and whether each entry is a function of axial position (x). For example, since there are i species and two electrodes, there are $2i$ unknown surface concentrations as functions of axial position. Note that there may be an arbitrary number, j, of electrode reactions.

The two flux expressions are the Fick's-law expression, which relates the flux to the gradient of concentration, and the Faraday's-law expression, which relates the flux to the partial current densities due to each of the j electrochemical reactions.

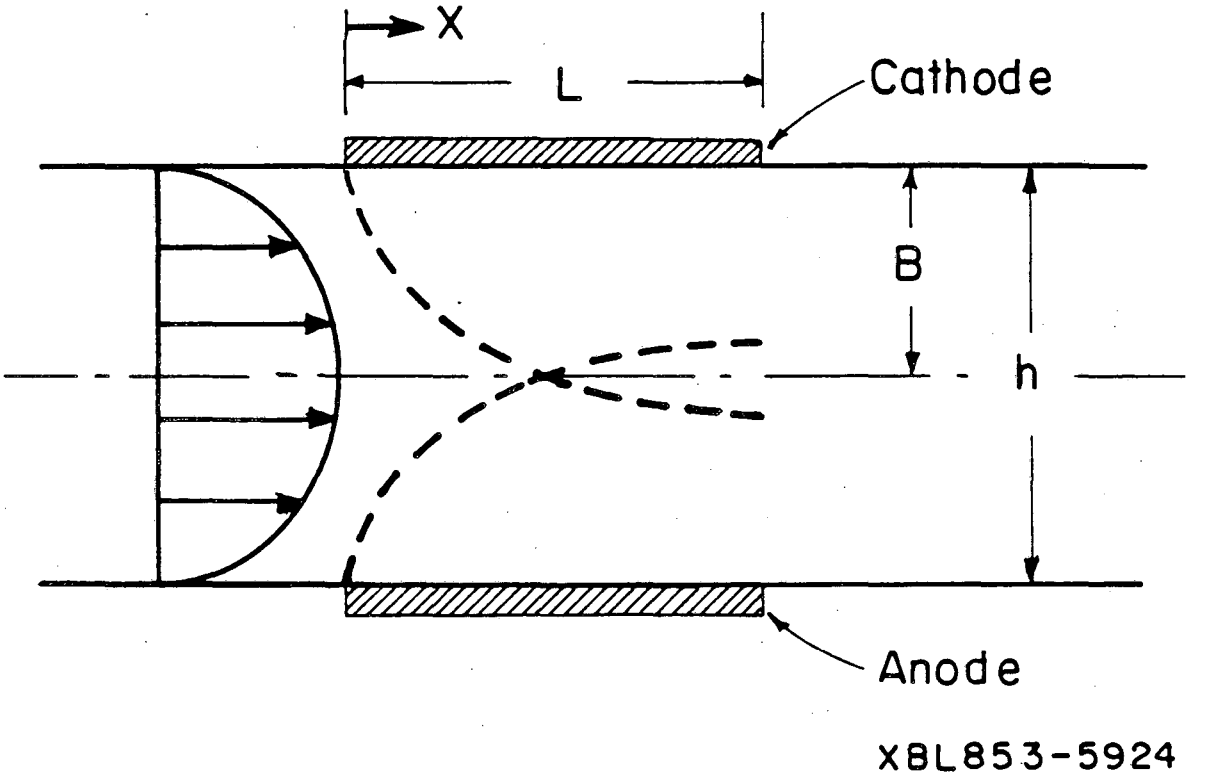

Figure 1. Cell geometry.

Table I Governing Equations

	Equations		Unknowns
$2i(x)$	Fick's Law	$2i(x)$	Fluxes
$2i(x)$	Faraday's Law	$2i(x)$	Surface Concentrations
$2j(x)$	Butler-Volmer	$2j(x)$	Partial Currents
$2j(x)$	Surface Overpotential	$2j(x)$	Surface Overpotentials
$2j(x)$	$U_{j,o}$	$2j(x)$	$U_{j,o}$
$2(x)$	$\Phi^o(x)$	$2(x)$	$\Phi^o(x)$
1	Equal Currents	1	Φ^*
$2(x)$	Total Currents	$2(x)$	Total Currents
1	Cell Potential	1	V_{anode}
1	Zero of Potential	1	$V_{cathode}$

The Fick's-law expression is written as a superposition integral and will be discussed in the next section ("Solution Technique"). The Faraday's-law expression, for a reaction of the form

$$\sum_i s_{ij}\, M_i^{z_i} \rightarrow n_j e^- , \qquad [1]$$

is written

$$N_i = -\sum_j \frac{s_{ij}\, i_j}{n_j F} , \qquad [2]$$

where s_{ij} is the stoichiometric coefficient of species i in reaction j, n_j is the number of electrons transferred in reaction j, and i_j is the partial current density due to reaction j.

The partial current density i_j is given by the Butler-Volmer expression, which describes the kinetics of each electrode reaction (10):

$$i_j = i_{o\,j} \left[\exp\left(\frac{\alpha_{a\,j} F}{RT} \eta_{s\,j} \right) - \exp\left(\frac{-\alpha_{c\,j} F}{RT} \eta_{s\,j} \right) \right], \qquad [3]$$

where $i_{o\,j}$ is the exchange current density for reaction j and depends on the surface concentrations c_{io}. This dependence is expressed as

$$i_{o\,j} = i_{oj,ref} \prod_i \left(\frac{c_{io}}{c_{i,ref}} \right)^{\gamma_{ij}} , \qquad [4]$$

where $i_{oj,ref}$ is the exchange current density evaluated at reference concentrations $c_{i,ref}$. The surface overpotential, $\eta_{s\,j}$ is defined as

$$\eta_{s\,j} = V - \Phi_o - U_{j,o} , \qquad [5]$$

where

$$U_{j,o} = \left[U_j^\theta - \frac{RT}{n_j F} \sum_i s_{ij} \ln\left(\frac{c_{io}}{\rho_o} \right) \right] - \left[U_{re}^\theta - \frac{RT}{n_{re} F} \sum_i s_{i,re} \ln\left(\frac{c_{i,re}}{\rho_o} \right) \right] . \qquad [6]$$

The subscript re denotes the reference electrode reaction, U_j^θ is the standard

electrode potential of reaction j, and Φ^o is the potential in the solution just outside the diffuse double layer. When there is excess supporting electrolyte, Φ^o is governed by Laplace's equation (11). The solution to Laplace's equation for an arbitrary current distribution is (12)

$$\Phi^o_{cath}(x) = \Phi^* - \frac{1}{2\pi\kappa_\infty}\left\{\int_0^L [i_{cath}(x')\ln[sinh^2(\pi\frac{x-x'}{2h})] + i_{an}(x')\ln[cosh^2(\pi\frac{x-x'}{2h})]dx'\right\}, \qquad [7]$$

The integration constant Φ^* has the physical significance of setting the relative amounts of total overpotential on the anode and cathode.

Another equation results from the condition that the currents on the two electrodes must be equal, where the currents are the integrals of the current densities which are the sums of the partial current densities due to the electrode reactions.

The final specifications are the cell current or potential and a zero of potential. In this problem formulation, the cell potential is specified, and the cell current is calculated.

The right column in table I shows the unknowns corresponding to the equations listed above.

It is convenient to write the equations listed in table I in dimensionless form, because fewer parameters are needed to define each problem. For a system with i species and j reactions, $(2 + 2ij + 4i + 4j)$ dimensionless parameters are needed. These are parameters characterizing the electrode reactions, the geometry, the transport properties, and the operating conditions. Table II lists these dimensionless parameters. The parameters J_j, N, and $Pe\ d_e/L$ are defined as follows:

Table II Dimensionless Parameters

Parameter	Significance	Number of Parameters
γ_{ij}	concentration dependence of exchange current	ij
$\dfrac{\alpha_{aj}}{-n_m/s_{Rm}}$	anodic transfer coefficient	j
$\dfrac{\alpha_{cj}}{-n_m/s_{Rm}}$	cathodic transfer coefficient	j
J_j	exchange current	j
$U_j^\theta\left(\dfrac{-n_m F}{s_{Rm} RT}\right)$	standard electrode potential	j
$\dfrac{\rho_o}{c_{R\alpha}}$	solvent density†	1
$\dfrac{c_{i,re}}{c_{R\alpha}}$	reference-electrode concentrations	i
$\dfrac{c_{i,ref}}{c_{R\alpha}}$	reference concentrations (for $i_{oj,ref}$)	i
$\dfrac{s_{ij} n_m}{s_{Rm} n_j}$	stoichiometric coefficients	$ij-1$
h/L	aspect ratio	1
$\dfrac{D_i}{D_R}$	diffusion coefficients	$i-1$

† This parameter is not dimensionless because it is used only in conjunction with U_j^θ. Since the value of U_j^θ depends on the units used to describe the primary reference state, such as molality, U_j^θ has not only units of volts, but also hidden units of molality.

N	dimensionless limiting current ‡	1
$V_{cell}\left(\frac{-n_m F}{s_{Rm} RT}\right)$	applied potential	1
$\frac{c_{i\infty}}{c_{R\infty}}$	feed concentrations	$i-1$
$Pe\ d_e / L$	dimensionless gap thickness (relative to boundary layer)	1
		$2 + 2ij + 4i + 4j$

‡ This interpretation holds only for thin diffusion boundary layers.

$$J_j = \frac{-n_m}{s_{Rm}} \left(\frac{FL}{RT\kappa_\infty} \right) i_{oj,ref} \ , \qquad [8]$$

$$N = \frac{n_m^2}{s_{Rm}^2} \frac{F^2 D_R c_{R\infty}}{RT\kappa_\infty} \left(\frac{6<v>L^2}{hD_R} \right)^{1/3} , \qquad [9]$$

$$Pe \ d_e / L = \frac{4h^2<v>}{D_R L} . \qquad [10]$$

Alternatively, $[N(Pe \ d_e/L)^{-1/3} \, h/L]$ could be specified instead of N. This parameter would represent the ratio of feed concentration to supporting electrolyte concentration because it would contain $c_{R\infty}/\kappa_\infty$, where, for excess supporting electrolyte, κ_∞ is proportional to the supporting-electrolyte concentration.

Solution Technique

The key to the numerical method for solving the coupled equations discussed above is the linearity of the convective diffusion equation. Only the boundary conditions are nonlinear. Therefore, Duhamel's superposition theorem (*e.g.* 13,14) may be used to reduce the two-dimensional problem to one-dimensional boundary integral equations.

By applying Duhamel's theorem to the convective diffusion equation in a channel, the flux of species i at an electrode is written in terms of surface concentrations only. No concentrations within the electrolyte are needed. This expression is, on the cathode (15),

$$N_{i,cath}(x) = -\frac{D_i}{B} \int_0^x \frac{dc_{i,cath}}{dx}\Big|_{x^*} C_\xi(\zeta-\zeta^*,-1) \, dx^* + \frac{D_i}{B} \int_0^x \frac{dc_{i,an}}{dx}\Big|_{x^*} C_\xi(\zeta-\zeta^*,1) \, dx^* , \qquad [11]$$

where

$$\xi = y'/B \qquad [12]$$

$$\zeta = x \frac{D_i}{\frac{3}{2}B^2 < v >}. \qquad [13]$$

On the anode, the electrode subscripts and signs are reversed. These integrals are discretized by the method of Acrivos and Chambré (16), which is based on a method suggested by Wagner (17). Note that the flux of species i on an electrode is affected by the behavior of both electrodes because the diffusion boundary layers can interact. Also note that the flux depends only on upstream concentrations because axial diffusion is negligible. The dimensionless fluxes $C_\xi(\zeta\text{-}\zeta^*,\text{-}1)$ and $C_\xi(\zeta\text{-}\zeta^*,1)$, discussed in reference 15, are solutions to the convective diffusion equation with a unit step change in concentration on one electrode. For the wall with the step change in concentration and $\zeta < 0.11$,

$$C_\xi(\zeta,-1) = -\frac{1}{2}(1.35659745\zeta^{-1/3} - 0.2 - 0.060733452\zeta^{1/3}), \qquad [14]$$

and

$$C_\xi(\zeta,-1) = -\frac{1}{2}(1 + 2\sum_{k=1}^{3} |A_k|\, e^{-\lambda_k^2\zeta}) \qquad [15]$$

for $\zeta \geq 0.11$, where

$$\begin{array}{ll} \lambda_1 = 1.6815953222 & A_1 = \ \ 0.8580866740 \\ \lambda_2 = 3.6722904 & A_2 = -0.65921993 \\ \lambda_3 = 5.6698573459 & A_3 = \ \ 0.5694628499\,. \end{array} \qquad [16]$$

For the wall without the step change,

$$C_\xi(\zeta,1) = -\frac{1}{2}(\exp\,(0.9594 - \frac{0.6069}{\zeta} - 0.4512e^{-0.276/\zeta})) \qquad [17]$$

for $\zeta < 0.18$ and

$$C_\xi(\zeta,1) = -\frac{1}{2}(1 - 2\sum_{k=1}^{3} A_k e^{-\lambda_k^2\zeta}) \qquad [18]$$

for $\zeta \geq 0.18$.

Figures 2 and 3 show the iterative scheme to solve the dimensionless form of the equations in table I. The basis of the scheme is to iterate on the potential distributions $\Phi^o_{an}(x)$ and $\Phi^o_{cath}(x)$. Figure 2 is a detailed picture of the order in

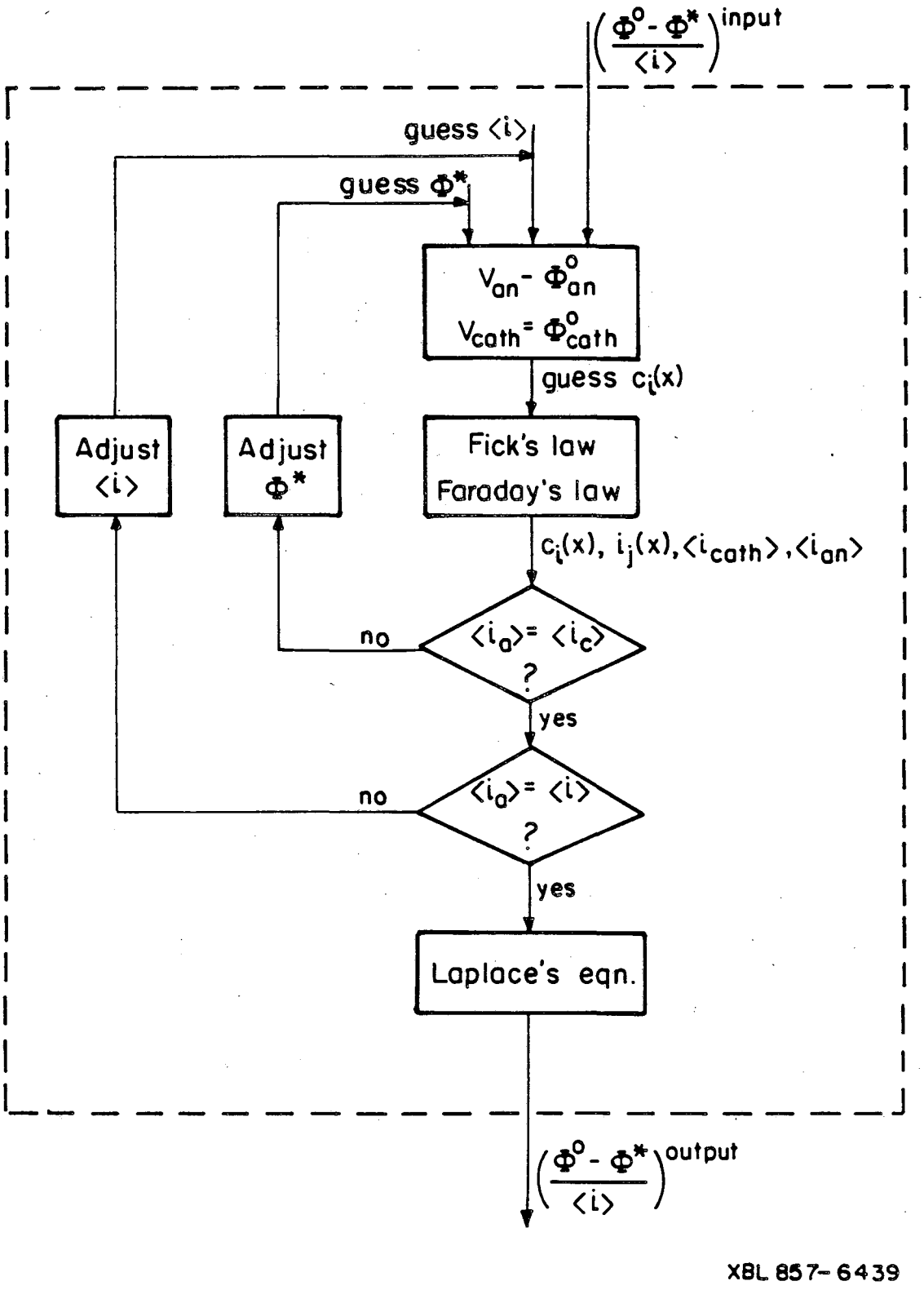

XBL 857-6439

Figure 2. Scheme for calculating a new potential distribution.

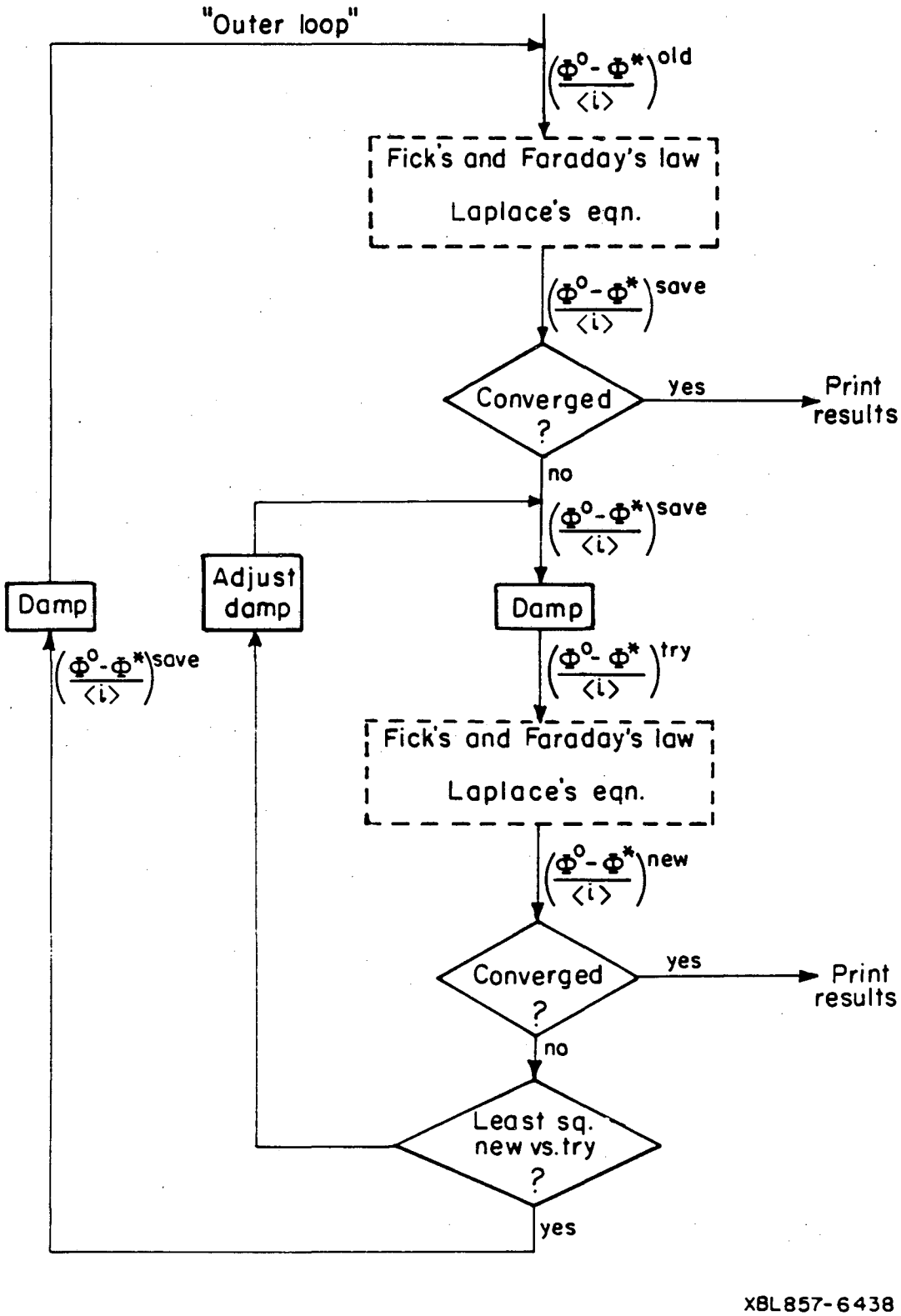

Figure 3. Damping scheme.

which the governing equations are solved, and figure 3 shows how the potential distributions are damped from iteration to iteration.

Before examining figure 2 in detail, one must first understand the physical significance of Φ^* and $<i>$. Note that, in equation 7, if one subtracts Φ^* from both sides and divides through by $<i>$, the left side is $(\Phi^o - \Phi^*)/<i>$, which represents the shape of the potential distribution, and the right side shows how this shape depends on the shape of the current distributions, $i/<i>$. The integration constant, Φ^*, in equation 7 sets the relative amounts of overpotential on the anode and cathode. For example, if Φ^* is too close to V_{an}, the overpotential $(V - \Phi^o)$ on the anode will be too low, and the integral of i_{an} will be less in magnitude than the integral of i_{cath}. Thus, Φ^* is adjusted to satisfy the condition that the currents are equal on the two electrodes. The average current, $<i>$, sets the magnitude of the overpotentials. For example, if $<i>$ is too high, the overpotentials calculated with the Φ^o from equation 7 will be small, and, hence, the currents calculated from these overpotentials will be too small to agree with the input $<i>$. In summary, $(\Phi^o - \Phi^*)/<i>$ describes the shape of the potential distribution, Φ^* determines the placement of Φ^o_{an} and Φ^o_{cath} relative to the electrode potentials, and $<i>$ sets the magnitude of $(V - \Phi^o)$.

We can now discuss the entire scheme of figure 2 in detail. Proceeding from top to bottom on figure 2, first, a guess is made for the potential distributions and for Φ^* and $<i>$.

The distributions $\Phi^o_{an}(x)$ and $\Phi^o_{cath}(x)$ are then substituted into the definition of surface overpotential (equation 5), which is, in turn, substituted into the Butler-Volmer kinetic expression (equation 3). The partial current densities i_j are then used in the Faraday's-law flux expression (equation 2). The resulting Faraday's-law expression, therefore, contains the guessed potential distribution and unknown surface concentrations (arising from the concentration dependence of the exchange current density). The Fick's-law expression also contains

unknown surface concentrations. By equating the Fick's-law and Faraday's-law expressions for the flux of each species on each electrode, one can obtain a set of equations to be solved for the unknown surface concentrations. These equations are solved by a multi-dimensional Newton-Raphson method at each axial mesh point, starting with the leading edge. The spacing of these mesh points is fine near the leading edge but coarser downstream, where the profiles are generally smooth. To speed the convergence of the Newton-Raphson method, the initial guesses for the surface concentrations are made by linearly extrapolating from the previous two axial positions. Let it be emphasized that the unknowns solved for simultaneously are the concentrations only at the present mesh point. Also, the electrodes do not interact at the present mesh point; rather the interaction propagates downstream from the already-solved mesh points.

After solving for the surface concentrations, Φ^* and $<i>$ are adjusted. Φ^* is adjusted to satisfy the condition that the currents are equal on the two electrodes. $<i>$ is adjusted so that the magnitude of the current on each electrode calculated from Fick's law and Faraday's law agrees with the magnitude of the current that was used in the solution to Laplace's equation (equation 7).

Then the new current distributions are substituted into Laplace's equation to calculate a new potential distribution. With the new potential distribution, one can check for convergence by comparing with the original guess. Unfortunately, the iteration on the potential distribution is unstable, and damping is necessary.

Figure 3 shows the details of the damping scheme. A damping factor is used to average the projected potential distribution with that from the previous iteration:

$$\Phi^o = damp * \Phi^o_{old} + (1-damp) * \Phi^o_{new}. \qquad [19]$$

To speed the convergence of this outer iteration loop, without producing instabilities, an optimum damping factor is chosen at each iteration. The optimum damping factor minimizes the mean square difference between the new potential

distribution obtained with the damping factor and the distribution that would result on the subsequent iteration if that damping were then removed.

Thus, in figure 3, the projected potential distribution is calculated and saved. This projected potential distribution is calculated by the scheme shown in figure 2 which is depicted by the dotted box in both figures 2 and 3.

Next, after checking for convergence, the optimum damping factor is sought. The lower part of figure 3 shows that a damping factor is applied to the saved distribution, and that damped distribution, denoted $(\Phi^o - \Phi^*)/<i>^{try}$, is input to the subsequent iteration to calculate $(\Phi^o - \Phi^*)/<i>^{new}$. When the sum-of-squares difference between $(\Phi^o - \Phi^*)/<i>^{try}$ and $(\Phi^o - \Phi^*)/<i>^{new}$ is a minimum, the optimum has been found.

When the optimum damping factor has been found, it is applied to the saved potential distribution, and the old potential distribution is updated.

Although a computer run can take more than 40 outer iterations and several hundred seconds on a CDC-7600 computer, the run time can be reduced to < 100 seconds by using previous runs to provide the initial guesses for the potential distributions. This technique is particularly effective when performing a series of runs to study the effects of a given parameter.

Single-Reaction Results

Since the effects of interacting boundary layers are most pronounced when mass transfer is controlling, only limiting-current results will be discussed. It is interesting that, for thick diffusion boundary layers, there is still a limiting current, even though products from the anode can diffuse to the cathode and react.

For simplicity, we shall consider a single electrode reaction and a single species, for example, a metal dissolution reaction on the anode and the metal plating reaction on the cathode. We shall also simplify the interpretation of the

results by considering a case with weak interaction of the electrodes through Laplace's equation ($h/L=1$). If the electrodes interact through Laplace's equation, the anode current distribution begins to resemble the cathode current distribution, as shown by Parrish and Newman (3). Thus, the source of interaction discussed here will be the diffusion of reacting species across the cell gap. After discussing the effect of interacting boundary layers, we shall discuss the effects of the axial component of current.

Figure 4 shows a dimensionless plot of the anode current distribution for three diffusion-boundary-layer thicknesses. The dimensionless gap thickness relative to the boundary-layer thickness is $Pe\ d_e/L$. For large $Pe\ d_e/L$ (≥ 100), for example high flow rates, the boundary layer is thin compared to the interelectrode gap. The current distributions shown in figure 4 resemble secondary current distributions because there are no mass-transfer limitations on the anodic dissolution reaction and because the cathode does not have much effect through Laplace's equation ($h/L=1$). Therefore the anodic current distribution is not strongly affected by the boundary-layer thickness.

The cathode, on the other hand, is mass transfer limited, and therefore i_{cath} is strongly dependent on $Pe\ d_e/L$. Figure 5 shows an example of the deviation of the cathode current distribution from the thin-boundary-layer result. (If $Pe\ d_e/L$ were 100 or higher, there would be no deviation, and the thin-boundary-layer approximation could be used.) In figure 5, the solid curve is the current density resulting from a step change in cathode surface concentration (from the feed concentration to zero) and a constant anode surface concentration ($c_{an}=c_{feed}$). This curve decays as $x^{-1/3}$ near the leading edge, where the boundary layer is thin, and levels off to a constant, where the concentration profile across the cell gap is linear (fully-developed mass transfer). The actual cathode current distribution, shown by the dotted line, decays as $x^{-1/3}$ near the leading edge, where the boundary layers are thin, but increases again when the anode

Anode Current Distribution

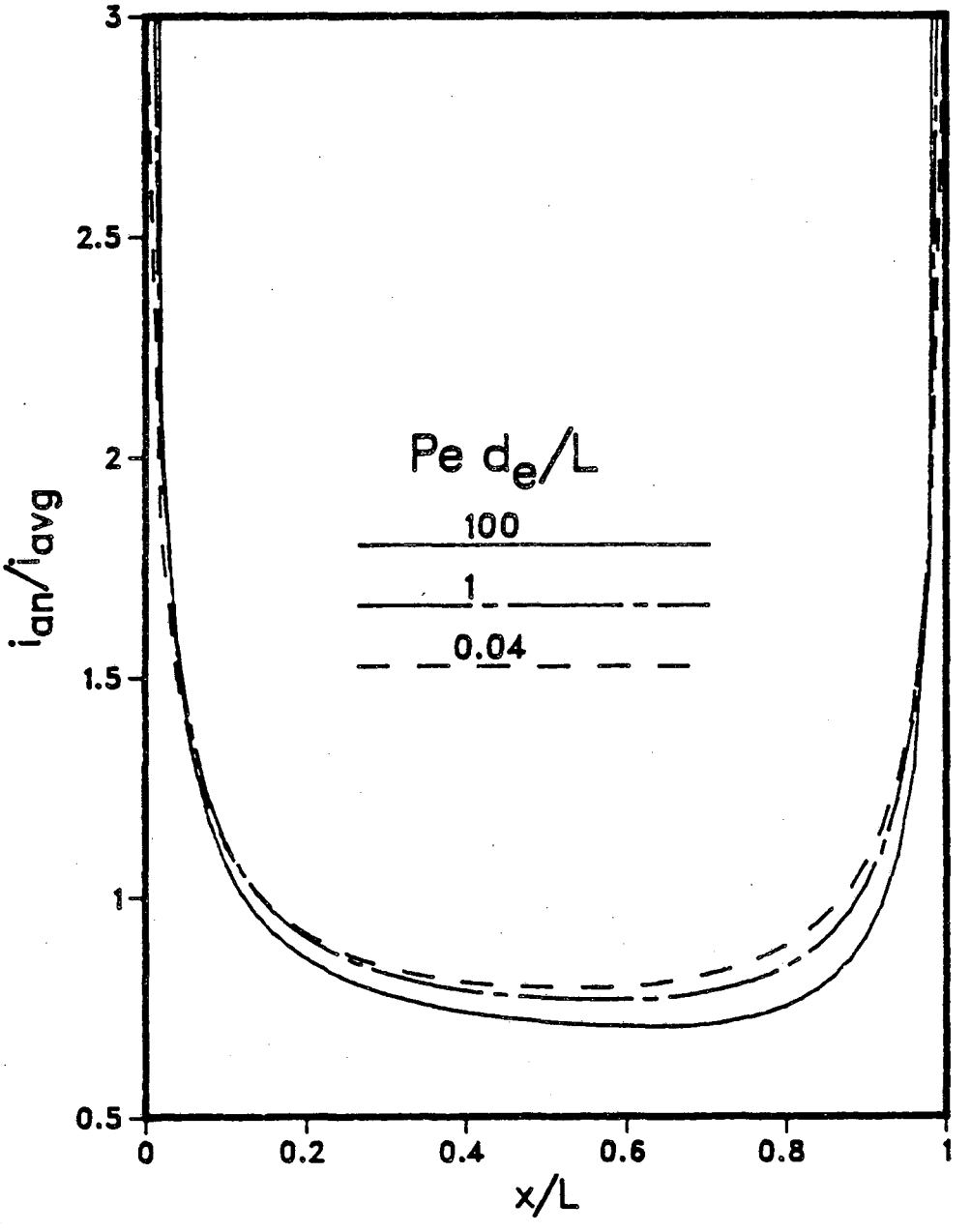

XBL 856-2902

Figure 4. Effect of boundary-layer thickness on anode current distribution.

Cathode Current Distribution

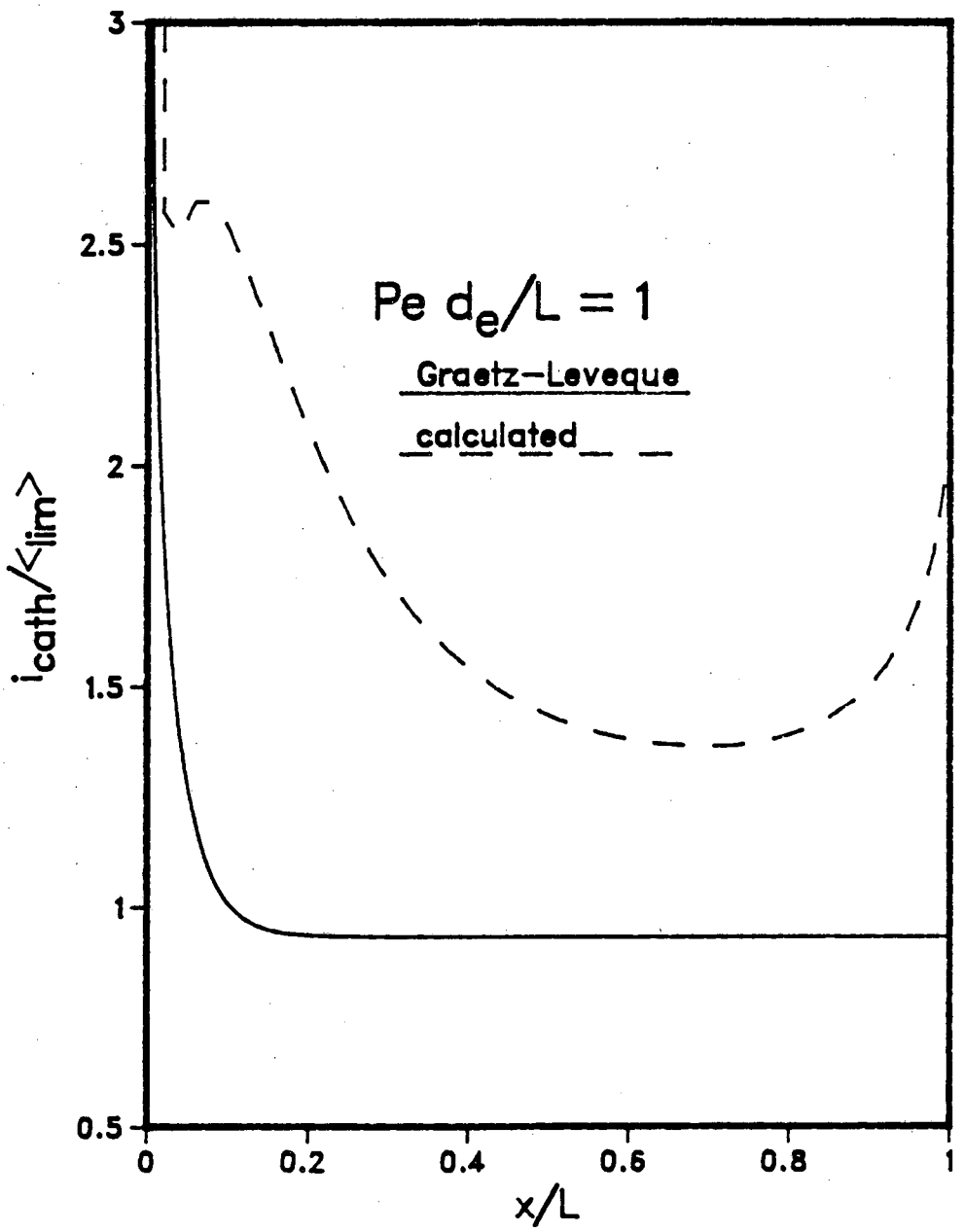

XBL 856-2897

Figure 5. Deviation from thin-layer approximation (normalized by average current from step-function problem).

boundary layer touches the cathode. That is, the solution near the cathode is no longer depleted because metal ions produced at the anode have diffused across the gap to the cathode. Away from the edges of the cell, the cathodic current density is low, roughly mirroring the behavior of the anode. Near the trailing edge, the anodic current density increases; therefore the cathodic current increases because some of the ions produced on the anode diffuse to the cathode.

We have seen how the interaction of the diffusion boundary layers affects the anodic and cathodic current distributions at the limiting current. Again, it is interesting that there is still a limiting current when the boundary layers interact. To understand why there is a limiting current and to understand the anode surface concentration profiles, one must examine the axial component of current.

Using the anodic and cathodic current distribution, one can calculate by a material balance the average current density flowing in the axial (fluid-flow) direction across a vertical cross-section at position x:

$$I_{axial}(x) = \frac{1}{L}\int_0^L [i_{an}(x') + i_{cath}(x')]dx'. \qquad [20]$$

Thus, negative axial currents indicate that there has been more cathodic reaction up to the axial position x. (Cathodic currents are negative.) Since the cathodic reaction depletes the solution of metal ions, the cup-mixing concentration at the position x is less than the feed concentration for negative axial currents. Figure 6 shows the axial current for $Pe\ d_e/L=1$. Note that the axial current is zero at $x=0$ and $x=L$ because there is no net flow of current beyond the electrode edges. The positive spike in I_{axial} near the leading edge results because the anodic current density rises more rapidly at the leading edge than the mass-transfer-limited cathodic current density (approximately $x^{-1/2}$ *vs.* $x^{-1/3}$). Throughout most of the cell, the extra current produced at the downstream edge of the anode flows upstream before reaching the cathode. Note that this does not mean that metal ions diffuse upstream, because in the bulk of

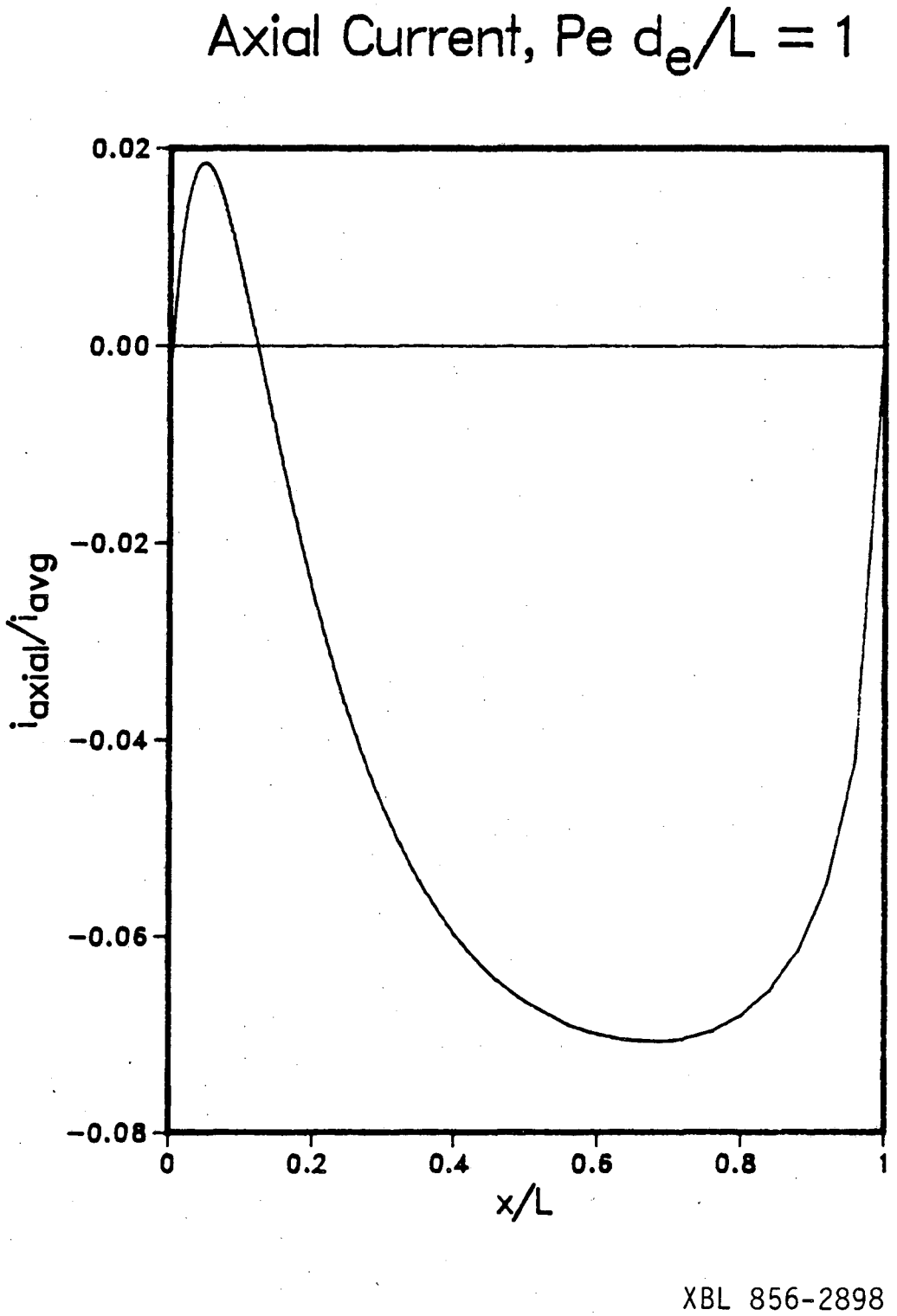

Figure 6. Axial current distribution for a thick boundary layer.

the solution, current flows by the migration of supporting-electrolyte ions.

The current and potential lines corresponding to figure 6 are shown in figure 7. The potential lines were calculated using the complete solution to Laplace's equation:

$$\Phi(x,y) = \Phi^{*} - \frac{1}{2\pi\kappa_{\infty}} \left\{ \int_0^L [i_{cath}(x') \ln [sinh^2(\pi \frac{x-x'}{2h}) + \sin^2(\pi \frac{y-h}{2h})] \right.$$

$$\left. + i_{an}(x') \ln [sinh^2(\pi \frac{x-x'}{2h}) + \sin^2(\pi \frac{y}{2h})] dx' \right\}, \qquad [21]$$

The current lines were plotted by starting at one electrode and stepping along a two-dimensional grid, numerically calculating the gradient of Φ at each x or y mesh point. In principle, it should be possible to obtain the same current lines starting on either electrode. However, since the results were slightly different, an average was taken.

The figures show that throughout most of the cell, the axial current is negative. Therefore, one would expect the electrolyte to be depleted throughout most of the cell. One can examine the depletion of the electrolyte by following the anodic surface concentration as a function of axial position. Since the surface concentration of metal ion is zero at the cathode (limiting current), when the anode surface concentration is twice the feed concentration, the cup-mixing concentration is roughly equal to the feed concentration. Figure 8 shows the anode surface concentration as a function of axial position. Note that the spike in c_{an}/c_{feed} above 2 corresponds to the positive spike in axial current. Further downstream, however, the solution is depleted because the axial current is negative; therefore c_{an}/c_{feed} is less than 2.

The effect of boundary-layer thickness is also shown in figure 8. As the diffusion boundary layer becomes thicker (lower flow rate), the electrolyte becomes more depleted. In fact, the anode surface concentration can fall below the feed concentration, as shown in figure 8.

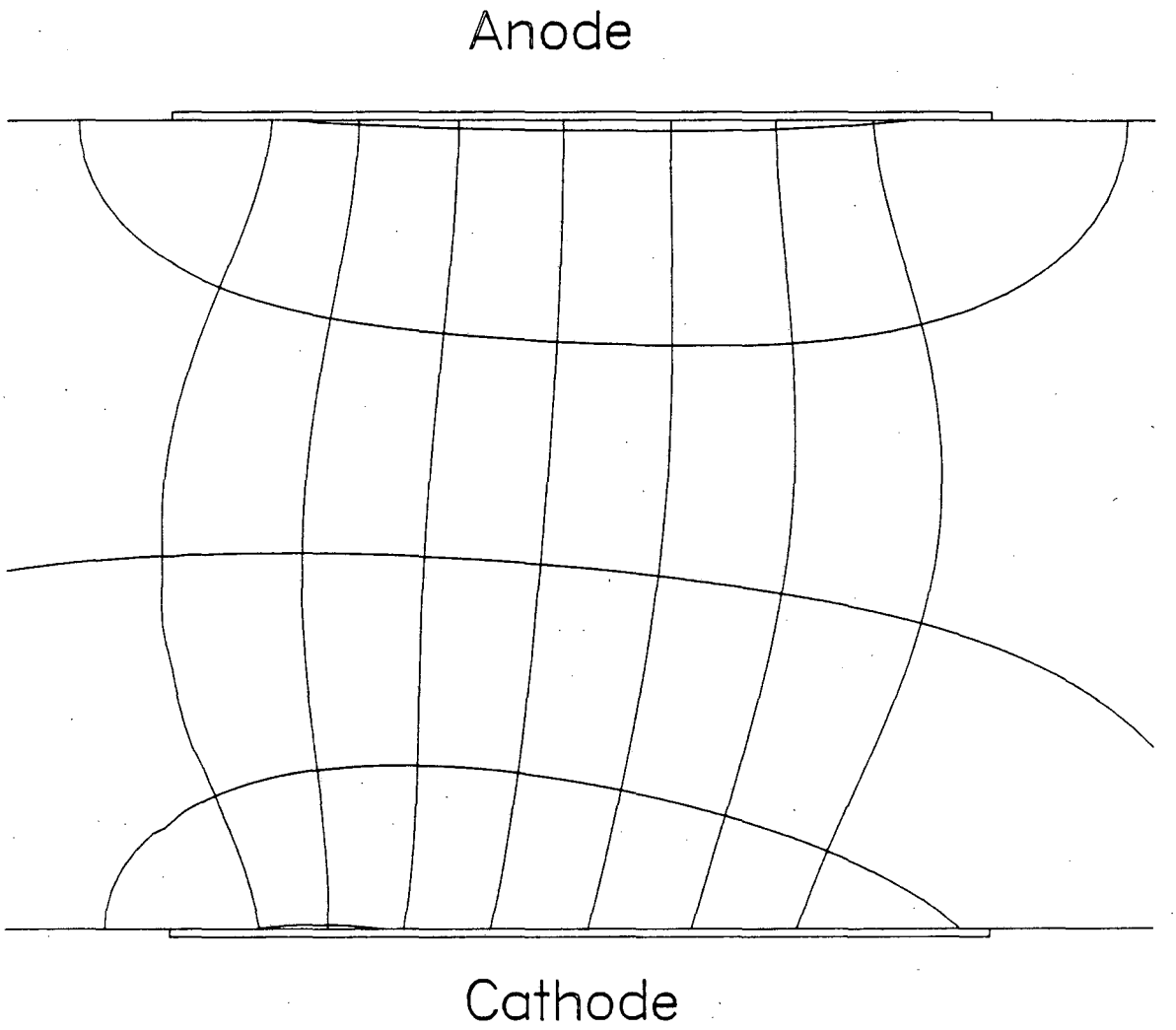

XBL 856-2901

Figure 7. Current and potential lines for a thick boundary layer.

Anode Surface Concentration

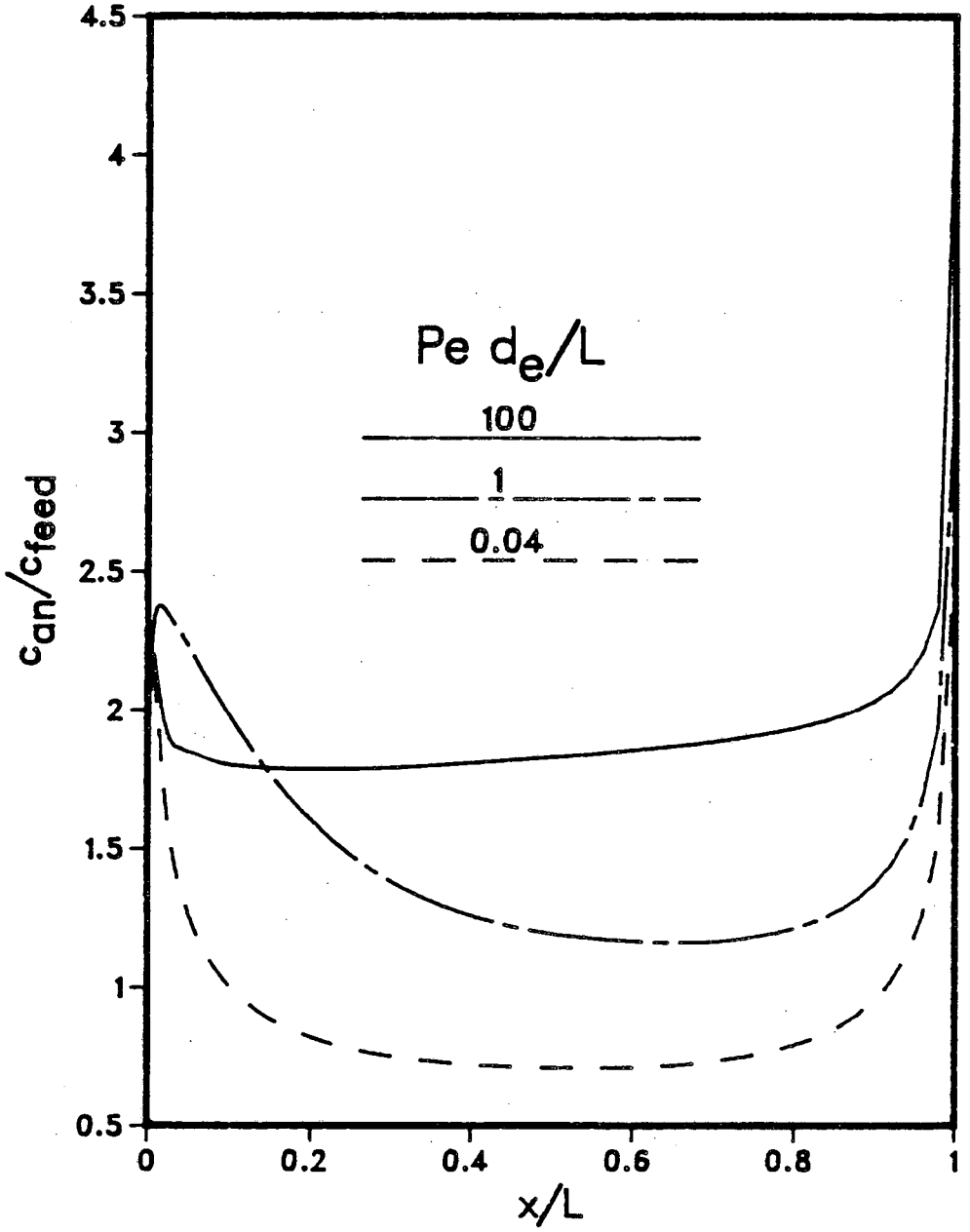

XBL 856-2899

Figure 8. Effect of boundary-layer thickness on anode surface concentration.

We can now discuss the presence of a limiting current for interacting boundary layers. At first, one might think that, by increasing the cell potential, the anode would produce more ions that would diffuse over to the cathode and react, and that, therefore, there would not be a limiting current. However, this is not the case because if c_{an} were much greater than $2c_{feed}$ everywhere, the axial current would be positive everywhere. Therefore, the production of metal ions on the anode is limited by the requirement that there be no net current flow beyond $x=L$. Another way of thinking about this is that the ions produced on the anode must travel some distance downstream before reaching the cathode. The ratio of the electrode length L to this distance is a rough indication of the amplification effect of ions reaching the cathode from the anode instead of just from the feed stream. This amplification factor can be large, but it is still finite, and there is still a limiting value for the current.

Conclusions

The effects of interacting diffusion boundary layers and of the axial component of current have been discussed for a channel flow cell. When $Pe\ d_e/L < 100$, the boundary layers interact and may not be considered thin. That is, if the gap is thin, the flow rate is low, the electrodes are long, or the diffusion coefficient is high, the electrodes may not be treated separately in the mathematical analysis.

An interesting result of the model is that there is a limiting current for thin gaps. Even though products from the anode can react on the cathode, the production of species on the anode is limited by the requirement of equal currents on the two electrodes.

The effect of axial currents is to deplete the electrolyte of metal ions throughout most of the cell. Thus, the two-dimensional structure of the potential distribution is important, and it should not be assumed that the current

lines travel straight across from one electrode to the other.

Although only single-reaction results were presented for an aspect ratio $h/L=1$, the model discussed here may be used to assess the effect of multiple reactions and of interaction between the electrodes through the potential distribution.

Acknowledgment

This work was supported by the Assistant Secretary for Conservation and Renewable Energy, Office of Energy Systems Research, Energy Storage Division of the U.S. Department of Energy under Contract No. DE-AC03-76SF00098.

Nomenclature

B	channel halfwidth, cm
c_{io}	surface concentration of species i, mol/cm^3
$C_\xi(\zeta-\zeta^*,-1)$	dimensionless flux on the electrode with a unit step change in concentration
$C_\xi(\zeta-\zeta^*,1)$	dimensionless flux on the electrode without the unit step change in concentration
d_e	equivalent diameter (=$2h$ for a channel), cm
D_i	diffusion coefficient of species i, cm^2/s
$damp$	damping factor (see equation 19)
F	Faraday's constant, 96,487 C/eq

h	interelectrode gap thickness, cm
$\langle i \rangle$	average current density, A/cm^2
i_j	current density due to reaction j, A/cm^2
$i_{0,j}$	exchange current density for reaction j, evaluated at the local surface concentrations, A/cm^2
L	electrode length, cm
N_i	flux of species i, mol/cm^2-s
R	universal gas constant, 8.3143 J/mol-K
T	absolute temperature, K
$\langle v \rangle$	average fluid velocity, cm/s
V	electrode potential, volts
x	axial coordinate, cm
y	normal coordinate, measured from the anode, cm
y'	normal coordinate, measured from center of channel, cm
z_i	charge number of species i

Greek

$\alpha_{a,j}$	anodic transfer coefficient for reaction j
$\alpha_{c,j}$	cathodic transfer coefficient for reaction j

γ_{ij}	exponent for concentration dependence of exchange current for reaction j on species i
η_{sj}	surface overpotential for reaction j, volts
κ_{∞}	conductivity of feed solution, $ohm^{-1}cm^{-1}$
Φ^{o}	potential in solution just outside diffuse double layer, volts
Φ^{*}	integration constant in equation 7 or 21, volts
ρ_{o}	pure solvent density, kg/cm^{3}
ζ	dimensionless axial coordinate defined in equation 13
ξ	dimensionless normal coordinate defined in equation 12

Subscripts

an	anode
$cath$	cathode
i	species in solution
j	electrode reaction
m	main reaction
o	electrode surface
R	principal reactant
re	reference electrode reaction

ref	reference concentrations at which exchange current density $i_{oj,ref}$ was measured
∞	feed solution

Superscripts

o	electrode surface

References

1. R. E. White, Mike Bain, and Mike Raible, "Parallel Plate Electrochemical Reactor Model," *Journal of the Electrochemical Society*, **130** (1983), 1037-1042.

2. W. R. Parrish and John Newman, "Current Distribution on a Plane Electrode below the Limiting Current," *Journal of the Electrochemical Society*, **116** (1969), 169-172.

3. W. R. Parrish and John Newman, "Current Distributions on Plane, Parallel Electrodes in Channel Flow," *Journal of the Electrochemical Society*, **117** (1970), 43-48.

4. Reinaldo Cabán and Thomas W. Chapman, "Rapid Computation of Current Distribution by Orthogonal Collocation," *Journal of the Electrochemical Society*, **123** (1976), 1036-1041.

5. George P. Sakellaropoulos, "Criteria for Selective Path Promotion in Electrochemical Reaction Sequences," *A.I.Ch.E Journal*, **25** (1979), 781-793.

6. George P. Sakellaropoulos and Gary A. Francis, "Electrochemical Reactor Analysis: Selectivity of Multiple Competing Reactions," *Journal of the Electrochemical Society*, **126** (1979), 1928-1937.

7. George P. Sakellaropoulos and Gary A. Francis, "Selectivity and Reactor Analysis for Parallel Electrochemical Reactions," *Journal of Chemical Technology and Biotechnology*, **30** (1980), 102-109.

8. Johnsee Lee and J. R. Selman, "Effects of Separator and Terminal on the Current Distribution in Parallel-Plate Electrochemical Flow Reactors," *Journal of the Electrochemical Society*, **129** (1982), 1670-1678.

9. Frank M. White, *Viscous Fluid Flow*, McGraw Hill, New York (1974).

10. John Newman, *Electrochemical Systems*, Prentice-Hall, Englewood Cliffs, New Jersey (1973).

11. Ralph Edward White, *Simultaneous Reactions on a Rotating Disk Electrode*, dissertation, University of California, Berkeley (March, 1977).

12. John Newman, "Engineering Design of Electrochemical Systems," *Industrial and Engineering Chemistry*, **60** (April, 1968), 12-27.

13. Francis B. Hildebrand, *Advanced Calculus for Applications, Second Edition*, pp. 463-466, Prentice-Hall, Englewood Cliffs, New Jersey (1976).

14. C. Ray Wylie, *Advanced Engineering Mathematics*, Fourth Edition, pp. 309-319, McGraw Hill, New York (1960).

15. Victoria Edwards and John Newman, "The Asymmetric Graetz Problem in Channel Flow," *International Journal of Heat and Mass Transfer*, **28** (1985), 503-505.

16. Andreas Acrivos and Paul L. Chambré, "Laminar Boundary Layer Flows with Surface Reactions," *Industrial and Engineering Chemistry*, **49** (June, 1957), 1025-1029.

17. Carl Wagner, "On the Numerical Solution of Volterra Integral Equations" *J. Math. Phys.*, **32** (1954), 289-301.

This report was done with support from the Department of Energy. Any conclusions or opinions expressed in this report represent solely those of the author(s) and not necessarily those of The Regents of the University of California, the Lawrence Berkeley Laboratory or the Department of Energy.

Reference to a company or product name does not imply approval or recommendation of the product by the University of California or the U.S. Department of Energy to the exclusion of others that may be suitable.

LAWRENCE BERKELEY LABORATORY
TECHNICAL INFORMATION DEPARTMENT
UNIVERSITY OF CALIFORNIA
BERKELEY, CALIFORNIA 94720